

This is an Open Access document downloaded from ORCA, Cardiff University's institutional repository: <https://orca.cardiff.ac.uk/id/eprint/177351/>

This is the author's version of a work that was submitted to / accepted for publication.

Citation for final published version:

Wu, Chuanshen, Zhou, Yue and Wu, Jianzhong 2025. Two-layer data-driven robust scheduling for industrial heat loads. *Journal of Modern Power Systems and Clean Energy* 13 (1) , pp. 265-275. 10.35833/MPCE.2024.000105

Publishers page: <http://dx.doi.org/10.35833/MPCE.2024.000105>

Please note:

Changes made as a result of publishing processes such as copy-editing, formatting and page numbers may not be reflected in this version. For the definitive version of this publication, please refer to the published source. You are advised to consult the publisher's version if you wish to cite this paper.

This version is being made available in accordance with publisher policies. See <http://orca.cf.ac.uk/policies.html> for usage policies. Copyright and moral rights for publications made available in ORCA are retained by the copyright holders.



# Two-Layer Data-Driven Robust Optimal Scheduling of Industrial Heating Loads

Chuanshen Wu, *Member, IEEE*, Yue Zhou, *Member, IEEE*, and Jianzhong Wu, *Fellow, IEEE*

**Abstract**—This study establishes a two-layer data-driven robust optimal scheduling approach to deal with the significant computational complexity and uncertainties in scheduling industrial heating loads, bitumen tanks (BTs). First, a two-layer deterministic optimal scheduling model is proposed to address the computational burden of utilizing flexibility from a large number of BTs. The key feature of this model is the capability to reduce the number of control variables through analyzing and modeling the clustered temperature transfer of BTs. Second, to tackle the uncertainties in the scheduling problem, historical data regarding BTs are collected and analyzed, and an unsupervised learning method is employed to construct the uncertainty set with convex boundaries and adjustable conservatism, based on which robust optimization can be conducted. The case results indicate that the proposed methods enable the utilization of flexibility in BTs, improving the level of onsite photovoltaic consumption and reducing the aggregated load fluctuation.

**Index Terms**—Bitumen tanks, demand response, industrial heating loads, robust optimization, uncertainty analysis.

## NOMENCLATURE

### Abbreviations

IHL	Industrial heating loads
BT	Bitumen tank
NP-hard	Non-deterministic polynomial-time hard
SVC	Support vector clustering
PLK	Piecewise linear kernel
PV	Photovoltaic

### Parameters

$P_{\text{absorb}}$	Heat absorb rate
$P_{\text{loss}}$	Heat loss rate
$P_{\text{net}}$	Heat transfer rate
$P_{\text{rate}}$	Rated heating power
$U$	Overall heat transfer coefficient
$A$	Area of a BT
$T$	Bitumen temperature
$T_{\text{amb}}$	Temperature of outside ambience
$c_v$	Heat capacity of the bitumen
$m$	Mass of the bitumen in a BT
$T_{\text{up}}$	Upper limit of bitumen temperature
$T_{\text{down}}$	Lower limit of bitumen temperature

$H$	Number of time slots in the time horizon
$N$	Number of BTs
$\Delta t$	Length of each time slot.
$\Delta T$	Magnitude of the gap
$\Delta T_{\text{up}}$	temperature increase in a $\Delta t$ period for a BT
$\Delta T_{\text{down}}$	temperature decrease in a $\Delta t$ period for a BT
$\zeta_m$	the $m^{\text{th}}$ slack variable
$\nu$	Regularization parameter
$\alpha/\beta$	Lagrange multiplier
$K$	Dimension of the historical data sample
$M$	Number of historical data samples
$U_m$	The $m^{\text{th}}$ historical data of $U$
$T_{\text{amb}}^m$	The $m^{\text{th}}$ historical data of $T_{\text{amb}}$
$Q$	Number of boundary support vectors

### State Variables

$T_{n,h}$	Temperature of $n^{\text{th}}$ BT at time $h$
$P_{\text{BL}}^h$	Base load of the industrial site at time $h$
$P_{\text{PV}}^h$	Power generation of local PV at time $h$
$\bar{T}_h$	Average temperature of BTs at time $h$
$\bar{T}_h^q$	Average temperature of BTs corresponding to the $q^{\text{th}}$ boundary support vector at time $h$ .

### Decision Variables

$x$	ON/OFF state of a BT
$x_{n,h}$	State of the $n^{\text{th}}$ BT at time $h$
$x_h$	Total number of BTs turned ON at time $h$

## I. INTRODUCTION

In the past decades, dispatchable loads have attracted vital attention due to their substantial potential for balancing power systems through management. In industrial sectors, industrial heating loads (IHLs) possess inherent operational flexibility due to their thermal storage capacity, enabling them to participate in demand response in power systems [1]. During the production processes of IHLs, a considerable amount of energy is required to maintain them within an appropriate temperature range for anytime use. Therefore, their efficient management suggests a significant opportunity for power system balancing [2].

In this paper, an industrial site with bitumen tanks (BTs) is researched as an example of IHLs. The global bitumen market was valued at around USD 105 billion in 2022, underscoring its substantial presence in the construction and infrastructure sectors worldwide [3]. In the UK, there are nearly 300 bitumen plants manufacturing over 20 million tonnes of bitumen annually [4]. To ensure the fluidity of bitumen for anytime use, BTs are needed to maintain the bitumen temperature within the required range. At present, there are mainly three heating methods for BTs,

Manuscript received: January 26, 2024; revised: April 2, 2024, and June 3, 2024; accepted: July 4, 2024.

This work was supported in part by the European Regional Development Fund through the Welsh Government under Grant 80835 (FLEXIS West) and by the EPSRC under Grant EP/W028573/1, EP/T022795/1 and EP/S018107/1 (SFSC2-203). (*Corresponding author: Yue Zhou.*)

The authors are with the School of Engineering, Cardiff University, Cardiff CF24 3AA, U.K. (e-mail: wuc23@cardiff.ac.uk; zhouy68@cardiff.ac.uk; wuj5@cardiff.ac.uk).

namely fuel heating, thermal oil heating, and electric heating [5]. Electric heating utilizes an electric resistance assembly to heat the bitumen in the tank, which is widely applied, especially in applications where precise temperature control of bitumen is essential. According to a survey conducted by MBA Asphalt Plant Co [6], one of the largest companies in the bitumen industry, electric BTs account for approximately 15% of the total market share of BTs worldwide, with around 65% of them being used in European countries. Moreover, considering that electric BTs are environmentally friendly due to the absence of combustion of fossil fuels, the proportion of electric BTs is anticipated to continue rising in the low-carbon-oriented future.

Electric BTs are typically equipped with electrical heating devices to maintain the bitumen within a certain temperature range, ensuring its fluidity for industrial applications in road construction, building infrastructure, petroleum, chemical, and various other fields [7]. By properly controlling the ON/OFF status of electrical switches, BTs act as thermal energy storage, providing the flexibility to respond to demand for the power grid. In recent years, there have been studies exploring the possibility of leveraging BTs to provide demand response services. For instance, researchers have developed control algorithms to alter the power consumption of BTs for real-time balancing between supply and demand in electric power systems [8]. Similar approaches have been applied to BTs for participating in enhanced frequency response within the Great Britain power system [9]. Existing studies have verified the significant potential of BTs to provide demand response and ancillary services to the grid.

Nowadays, for tapping the demand response potential of IHLs, there are mainly two research challenges. First, the scheduling of IHLs presents a significant computational challenge due to the strong nonlinearity and large number of integer variables involved [10]. This is a non-deterministic polynomial-time hard (NP-hard) problem with significant calculational complexity, and thus challenging. Second, the heating transfer rate of IHLs is nonlinear over time and easily affected by uncertainties, such as equipment parameters and environmental conditions [11]. Moreover, both model and data uncertainties propagate over time, making the scheduling of IHLs challenging to handle. The optimal scheduling of BTs is confronted with the aforementioned computational complexity and uncertainties issues. First, the optimal scheduling of the ON/OFF status of BTs is a complex integer programming problem. Second, since BTs are generally placed in the open air of an industrial site [12], the temperature change rate of a BT is easily influenced by weather conditions, such as temperature of outside ambience. This could lead to the day-ahead schedule cannot be implemented in reality.

Currently, exact methods and heuristic algorithms serve as the two primary categories of strategies to address the NP-hard problems. Many scholars have conducted extensive research on exact methods aimed at enhancing the solving efficiency of the NP-hard problems, including cutting plane-based methods [13], branch and bound-based methods [14], and methods based on Lagrange relaxation [15]. In addition, integer programming solvers, such as CPLEX and Gurobi, can automatically select

and apply suitable exact methods to solve NP-hard problems, which are widely used in industry and academia [16]. However, while exact methods guarantee the global optimum, they may become impractical for large or complex problems due to their high computational demands. To solve the NP-hard problems in a more efficient manner, heuristic algorithms are generally employed. However, a major limitation of heuristic algorithms is that the optimality cannot be guaranteed [17]. Moreover, for all the aforementioned methods, solving efficiency decreases with the increasing scale of the NP-hard problems.

To address the calculation complexity arising from a large number of BTs and attain the optimal solution, a two-layer control model is established in this paper, which decomposes a control problem into two hierarchical layers of sub-problems [18]. The upper-layer control reduces the scale of the model by clustering the control objects to decrease the number of control variables. The lower-layer control distributes the upper-layer control commands to each control object. For instance, a two-layer clustering algorithm is developed in [19] to improve the computing efficiency of coordinated scheduling for electric vehicles in multi-microgrid systems. The authors in [20] controlled the electric devices by aggregating them with similar physical properties to provide ancillary services and promote supply-demand balance. The authors in [21] introduced a clustering control approach for controllable household loads management, aimed at reducing peak consumption and achieving appropriate economic benefits. However, we have found no research focusing on the clustered analysis of IHLs, like BTs, for expedited scheduling purposes. This is because the temperature transfer process of BTs is nonlinear over time, and the temperature distribution in the population of BTs is discrete, leading to the analysis of clustered temperature transfer characteristics, especially in terms of average temperature constraint, challenging.

Moreover, to the best of the author's knowledge, there have been no studies considering the impact of external uncertainty factors on the temperature change rate of BTs in scheduling processes. To cope with uncertainties, robust optimization is widely used, which is a mathematical method aiming to develop models that generate solutions that are less sensitive to the uncertainties [22]. Previous studies typically describe uncertainty distributions using geometric shapes, such as box [23], ellipse [24], and polygon [25], which exhibit symmetrical spreading from the center. Therefore, they often encounter issues related to over-conservatism and reliance on a priori domain-specific knowledge. In real-world problems, uncertainty distributions can be extremely complex and challenging to accurately capture through the traditional shapes. Therefore, applying a technique that can adaptively construct the uncertainty set while adjusting the level of conservatism is highly valuable. In this paper, support vector clustering (SVC) [26] is adopted to construct the uncertainty set due to its ability to capture uncertainties more flexibly based on the real historical data. Notably, the partial derivatives of the bitumen temperature with respect to the external uncertainty factors are derived to ensure that each element of the historical data samples has the same unit for the SVC implementation.

Meanwhile, to address the computational burden caused by the soft margins of uncertain sets, a piecewise linear kernel (PLK) [27] is introduced in the SVC technique to approximate the uncertainty sets as convex polyhedrons. The implementation of the PLK-based SVC technique enables the flexible adjustment of the conservatism of the uncertainty set by modifying the regularization parameter. This adjustment is crucial for achieving the balance between the robustness and performance of the optimization results.

The main contributions of this paper are provided as follows.

- 1) The clustered temperature transfer characteristics of BTs are investigated with the aim of accelerating scheduling.
- 2) A two-layer optimal scheduling model is proposed to speed up the solution efficiency for the scheduling of BTs. In this model, the number of control variables is significantly reduced and remains unaffected by the increasing scale of BTs.
- 3) A data-driven PLK-based SVC technique is developed to deal with the uncertainties in the two-layer robust optimal scheduling of BTs. The shape of the uncertainty set can be adaptively constructed, and the level of its conservatism can be flexibly adjusted.

The remainder of the paper is arranged as follows. Section II introduces the modeling and control of industrial BTs. Section III devises the two-layer optimization problem for scheduling industrial BTs. Section IV develops the two-layer model into a robust optimization format to deal with the uncertainties. Section V discusses the simulation results. Finally, Section VI concludes this paper and presents the future directions.

## II. MODELLING AND CONTROL OF BITUMEN TANKS

### A. Industrial Sites

As shown in Fig. 1, an industrial site with BTs, base load and onsite power generation can be treated as a microgrid connected to the power grid. In this industrial site, the participation of BTs in demand response is of great significance to accommodate onsite photovoltaic (PV) generation and reduce the impact of peak load on the power grid.

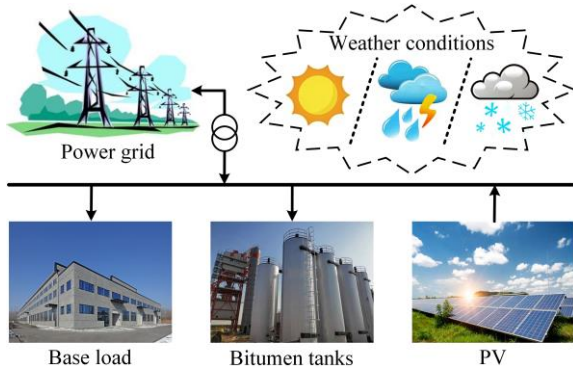


Fig. 1. An industrial site of BTs with base load and onsite PV generation.

### B. Temperature Control of Bitumen Tanks

To ensure the availability of bitumen, it is necessary to keep it in BTs in a liquid state and, simultaneously, ensure that its temperature is within an allowable range [12]. When the electrical switch of an industrial BT is turned ON, the heating

system is activated, causing the bitumen temperature to rise. Conversely, it naturally decreases when the electrical switch is turned OFF. Mathematically, the relationship between the heat transfer process of a BT and the ON/OFF state ( $x$ ) of its heater is given below:

$$P_{\text{net}} = P_{\text{absorb}} - P_{\text{loss}} = P_{\text{rate}} \times x - U \times A \times (T - T_{\text{amb}}) \quad (1)$$

In (1),  $x$  equals 1 if the heater is switched ON and 0 if OFF. Meanwhile,  $P_{\text{net}}$  decides the temperature change rate within the BT, as presented below:

$$P_{\text{net}} = c_v \times m \times \frac{dT}{dt} \quad (2)$$

By combining (1) and (2), the temperature change rate of the BT can be represented by its switching state:

$$\frac{dT}{dt} = \frac{P_{\text{rate}} \times x}{c_v \times m} - \frac{U \times A \times (T - T_{\text{amb}})}{c_v \times m} \quad (3)$$

Equation (3) shows that the rate of temperature change is also related to the current temperature of bitumen, so it is constantly changing, even with the same switching state.

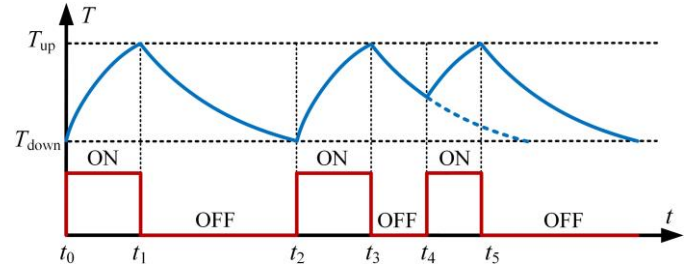


Fig. 2. Temperature control process of a BT.

Fig. 2 illustrates the temperature control process of a BT. The bitumen temperature rises when the heater is activated, while it decreases when the heater remains OFF. In Fig. 2, the electrical heater is set to be automatically turned OFF when the bitumen temperature touches the upper limit  $T_{\text{up}}$  at time  $t_{1/3/5}$ , while automatically turned ON when the bitumen temperature reaches the lower limit  $T_{\text{down}}$  at time  $t_2$ . Moreover, the heater can also be manually switched ON/OFF at any chosen time (e.g.,  $t_4$ ).

## III. TWO-LAYER DETERMINISTIC OPTIMAL SCHEDULING MODEL

### A. Original Optimal Scheduling Model

The objective of this study is to minimize the peak-to-valley difference of the electricity exchange between the industrial site and the external power grid:

$$\min f = \max_{1 \leq h \leq H} \left( \sum_{n=1}^N x_{n,h} \times P_{\text{rate}} + P_{\text{BL}}^h - P_{\text{PV}}^h \right) - \min_{1 \leq h \leq H} \left( \sum_{n=1}^N x_{n,h} \times P_{\text{rate}} + P_{\text{BL}}^h - P_{\text{PV}}^h \right) \quad (4)$$

The temperature transfer constraint of each BT and the limit of temperature in each BT are given as follows:

$$T_{n,h} = T_{n,h-1} + \frac{P_{\text{rate}} \times x_{n,h} - U \times A \times (T_{n,h-1} - T_{\text{amb}})}{c_v \times m} \times \Delta t, \forall n, \forall h \quad (5)$$

$$T_{\text{down}} \leq T_{n,h} \leq T_{\text{up}}, \forall n, \forall h \quad (6)$$

The original optimal scheduling model presented above is an integer programming problem, with the number of control variables being  $N \times H$ . Therefore, the solution time grows exponentially as the number of BTs increases.

### B. Two-Layer Optimal Scheduling Model

To deal with the computational burden as the number of BTs increases, a two-layer optimal scheduling model is proposed.

#### 1) Upper-Layer Clustered Optimization

The upper-layer clustering optimization aims to decide the total number of BTs turned ON at each time slot, by contrast to deciding the ON/OFF status of each individual BT in the original optimal scheduling model. Therefore, the number of decision variables is much reduced and does not change with the increasing numbers of BTs.

In this layer, the objective is formulated as:

$$\min f = \max_{1 \leq h \leq H} (x_h \times P_{\text{rate}} + P_{\text{BL}}^h - P_{\text{PV}}^h) - \min_{1 \leq h \leq H} (x_h \times P_{\text{rate}} + P_{\text{BL}}^h - P_{\text{PV}}^h) \quad (7)$$

Accordingly, the constraints of all the individual BT are also replaced by the constraints specifying the change of average temperature of the whole BT population (i.e., the clustered temperature transfer process). Specifically, by summing (5) of each BT and calculating the mean, the constraint for the average temperature of the entire BT population is given below:

$$\bar{T}_h = \bar{T}_{h-1} + \frac{P_{\text{rate}} \times \bar{x}_h - U \times A \times (\bar{T}_{h-1} - T_{\text{amb}})}{c_v \times m} \times \Delta t, \forall h \quad (8)$$

The temperatures of BTs are actually discretely distributed around the average temperature. To ensure that the temperature of each BT does not go beyond the upper/lower limit ( $T_{\text{up/down}}$ ), a certain gap needs to be kept between the average temperature of BTs and  $T_{\text{up/down}}$ , that is:

$$T_{\text{down}} + \Delta T \leq \bar{T}_h \leq T_{\text{up}} - \Delta T, \forall h \quad (9)$$

Remark: the control variables of this upper-layer clustered optimization model are  $\{x_h\}_{h=1}^H$ . The total number of these control variables is  $H$ , which will not be influenced by the number of BTs. Therefore, compared to the original optimal scheduling model, the calculation time can be significantly reduced when dealing with a large number of BTs.

#### 2) Lower-Layer State Distribution

Based on the obtained upper-layer optimization results, the lower-layer state distribution aims to decide which specific BTs are turned ON at each time slot. Basically, it should be satisfied that the total number of BTs turned ON after state distribution equals the obtained upper-layer optimization results:

$$x_h = \sum_{n=1}^N x_{n,h}, \forall h \quad (10)$$

However, there are many feasible state distribution results under the satisfaction of (10). Therefore, this study proposes a lower-layer state distribution principle, where BTs with lower

temperatures are preferentially turned ON at any time step. This ensures that the temperature of each BT remains as far from the temperature limits of  $T_{\text{up}}$  and  $T_{\text{down}}$  as possible.

$$\min f = \frac{1}{N} \sum_{n=1}^N (T_{n,h} - \bar{T}_h)^2, \forall h \quad (11)$$

s.t. (5), (6), (10)

Mathematically, the state distribution principle is equivalent to minimizing the variance of temperatures of BTs at different time periods, as presented above.

### C. Analysis of the Magnitude of the Gap

In this subsection, a detailed analysis is provided to acquire the magnitude of the gap  $\Delta T$  in (9). For a population of BTs, two arbitrary BTs are taken out for analysis. Based on the lower-layer state distribution, there are three combinations of the ON/OFF states for the two BTs at any time step: Scenario 1 – both BTs in the ON state, Scenario 2 – both BTs in the OFF state, and Scenario 3 – the BT with a lower temperature in the ON state while the BT with a higher temperature in the OFF state.

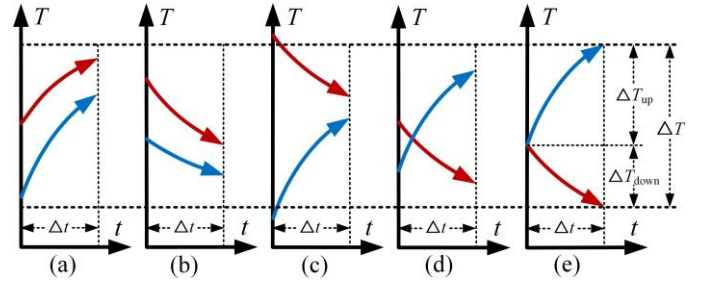


Fig. 3. The temperature transfer process of the two BTs.

In Scenario 1, the BT with a lower temperature will heat up faster, according to (5) and as shown in Fig. 3(a). In Scenario 2, the BT with a higher temperature will cool down faster, according to (5) and as shown in Fig. 3(b). Hence, in both Scenarios 1 and 2, the temperature difference between the two BTs will narrow down after the subsequent time slot. In Scenario 3, assuming that the absolute value of the initial temperature difference between the two BTs is  $\Delta T_{\text{initial}}$ . If  $\Delta T_{\text{initial}} \geq \Delta T$ , the temperature difference will narrow down after the subsequent time slot, as shown in Fig. 3(c). On the contrary, if  $\Delta T_{\text{initial}} < \Delta T$ , the temperature difference may increase after the subsequent time slot, as shown in Fig. 3(d). From Fig. 3(d), it can be deduced that the maximum temperature difference between the two BTs after the subsequent time slot occurs when  $\Delta T_{\text{initial}} \approx 0$ , as depicted in Fig. 3(e). The value of this maximum temperature difference between the two BTs is represented as  $\Delta T$ , derived by:

$$\Delta T = \Delta T_{\text{up}} + \Delta T_{\text{down}} = \frac{P_{\text{rate}} - U \times A \times (T_{1,h} - T_{\text{amb}})}{c_v \times m} \times \Delta t + \frac{U \times A \times (T_{2,h} - T_{\text{amb}})}{c_v \times m} \times \Delta t \approx \frac{P_{\text{rate}} \times \Delta t}{c_v \times m} \quad (12)$$

where  $\Delta T_{\text{up}}$  is the temperature increase in the next  $\Delta t$  period for the BT with initial temperature  $T_{1,h}$ , and  $\Delta T_{\text{down}}$  is the temperature decrease for the BT with initial temperature  $T_{2,h}$ . For the two

BTs,  $T_{1,h}$  is less than and infinitely approaches  $T_{2,h}$ , i.e.,  $T_{1,h} \approx T_{2,h}$ ; hence,  $\frac{U \times A \times (T_{2,h} - T_{1,h})}{c_v \times m} \approx 0$ , and therefore  $\Delta T \approx \frac{P_{\text{rate}} \times \Delta t}{c_v \times m}$ .

Summarizing Scenarios 1-3, it can be deduced that if  $\Delta T_{\text{initial}} < \Delta T$ , then the temperature difference between the two BTs after the subsequent time slot must be less than  $\Delta T$ . Thus, as long as the very initial width of the temperature distribution of the BT population before the first time step is smaller than  $\Delta T$ , it will not exceed  $\Delta T$  at any time step. Therefore, the value of  $\Delta T$  can be treated as the magnitude of the gap in (9). When the constraint (9) is respected and the lower-layer state distribution is applied, the temperature of each individual BT will not go beyond the temperature limits throughout the scheduling horizon.

To conclude the formulation, the objective of the upper-layer clustered optimization is (7), which is subject to the constraints of (8), (9), and (12). After the upper-layer clustered optimization, the total number of ON switching states at each time step can be calculated, and then the lower-layer state distribution is executed. The objective of lower-layer state distribution is (11), which is subject to the constraints of (5), (6), and (10).

#### IV. TWO-LAYER DATA-DRIVEN ROBUST OPTIMAL SCHEDULING MODEL

##### A. Uncertainty Analysis

The uncertainties of BTs lie in their clustered temperature transfer process. According to (8), there are two uncertain factors that influence the temperature change rate of BTs at an industrial site, specifically  $U$  and  $T_{\text{amb}}$ . For example, the  $U$  would be higher in rainy and snowy weather while lower in sunny and dry weather. In addition, there are also forecasting errors for  $T_{\text{amb}}$ . Unlike the uncertainties of PV and base load, the uncertainties of BTs may cause automatic ON/OFF switching of their electrical heaters, leading to significant deviations in the actual clustered temperature transfer process of BTs from the day-ahead schedule. This can result in fluctuations in the actual power consumption curve of BTs, deteriorating the execution results, which will be discussed in detail in Section V-B.

##### B. SVC-based Uncertainty Set Construction

To deal with the uncertainty of  $U$  and  $T_{\text{amb}}$  by using the robust optimal scheduling method, it is necessary to construct a convex two-dimensional uncertainty set for them.

###### 1) Data-driven SVC Technique

In specific, assuming that  $M$  historical data samples  $\{\mathbf{u}_m\}_{m=1}^M$  of the uncertain parameters considered are available, the objective of the SVC model is to seek a sphere that tries to enclose all the data samples with minimal volume and acts as the uncertainty set [28]:

$$\min_{R, \xi} R^2 + \frac{1}{M\nu} \sum_{m=1}^M \xi_m \quad (13)$$

$$s.t. \quad \|\phi(\mathbf{u}_m) - \mathbf{P}\|^2 \leq R^2 + \xi_m, \forall m \quad (14)$$

where  $\mathbf{P}$  is the center of the sphere (i.e., the uncertainty set);  $R$  is the radius of the sphere;  $\{\xi_m\}_{m=1}^M > 0$  are the slack variables adapted as the soft margins to accommodate outliers of

historical data samples;  $\nu > 0$  is the regularization parameter used to penalize outliers;  $\mathbf{u}_m$  is the  $m^{\text{th}}$  historical parameter sample (the elements in  $\mathbf{u}_m$  need to have the same unit);  $\phi(\cdot)$  is a mapping function for achieving transformation from low-dimensional to high-dimensional space, and is designed to facilitate the enclosure of  $\{\mathbf{u}_m\}_{m=1}^M$ .

For solving the above SVC model, it is reformulated into a Lagrange function [29]:

$$L(\mathbf{P}, R, \xi, \alpha, \beta) = R^2 + \frac{1}{M\nu} \sum_{m=1}^M \xi_m - \sum_{m=1}^M \alpha_m \left( R^2 + \xi_m - \|\phi(\mathbf{u}_m) - \mathbf{P}\|^2 \right) - \sum_{m=1}^M \beta_m \xi_m \quad (15)$$

To solve (15), the following Karush-Kuhn-Tucker (KKT) conditions [30] should be met:

$$\frac{\partial L}{\partial R} = 0 \rightarrow \sum_{m=1}^M \alpha_m = 1 \quad (16)$$

$$\frac{\partial L}{\partial \mathbf{P}} = \mathbf{0} \rightarrow \mathbf{P} = \sum_{m=1}^M \alpha_m \phi(\mathbf{u}_m) \quad (17)$$

$$\frac{\partial L}{\partial \xi_m} = 0 \rightarrow \alpha_m + \beta_m = \frac{1}{M\nu} \quad (18)$$

Putting the KKT conditions into (15), the dual problem [31] can be obtained below:

$$\min_{\alpha} \sum_{i=1}^M \sum_{j=1}^M \alpha_i \alpha_j \phi(\mathbf{u}_i)^T \phi(\mathbf{u}_j) - \sum_{i=1}^M \alpha_i \phi(\mathbf{u}_i)^T \phi(\mathbf{u}_i) \quad (19)$$

$$s.t. \quad 0 \leq \alpha_m \leq \frac{1}{M\nu}, \forall m \quad (20)$$

$$\sum_{m=1}^M \alpha_m = 1 \quad (21)$$

Generally, to construct a convex two-dimensional uncertainty set, it is necessary to give the mapping function  $\phi(\cdot)$ . However, in nonlinear classification problems, obtaining the appropriate mapping function from low-dimensional to high-dimensional space may be challenging, and sometimes even infeasible [32].

In this paper, the kernel function  $K(\cdot, \cdot)$  is adopted to address this issue. Kernel function can solve the nonlinear classification problem in the low-dimensional space without explicitly giving the mapped function [33]. Here, the PLK is selected as the kernel trick to facilitate solving the above dual problem, which implicitly calculates the inner product between data points in (19) as follows [27]:

$$K(\mathbf{u}_i, \mathbf{u}_j) = \phi(\mathbf{u}_i)^T \phi(\mathbf{u}_j) = \sum_{k=1}^K \min\{u_i^k, u_j^k\} \quad (22)$$

where  $u_{i/j}^k$  is the  $k^{\text{th}}$  element of  $\mathbf{u}_{i/j}$ .

After calculating the dual problem, the related correlations of the results are described below [26]:

$$\|\phi(\mathbf{u}_m) - \mathbf{P}\|^2 = \begin{cases} > R^2, & \text{if } \alpha_m = \frac{1}{Mv} \text{ and } \beta_m = 0 \\ = R^2, & \text{if } 0 < \alpha_m < \frac{1}{Mv} \text{ and } 0 < \beta_m < \frac{1}{Mv}, \quad \forall m \\ < R^2, & \text{if } \alpha_m = 0 \text{ and } \beta_m = \frac{1}{Mv} \end{cases} \quad (23)$$

where  $\|\phi(\mathbf{u}_m) - \mathbf{P}\|^2 > R^2$  indicates the  $\mathbf{u}_m$  is an outlier outside the convex uncertainty set;  $\|\phi(\mathbf{u}_m) - \mathbf{P}\|^2 = R^2$  indicates the  $\mathbf{u}_m$  is a boundary support vector, which forms the boundaries of the convex uncertainty set;  $\|\phi(\mathbf{u}_m) - \mathbf{P}\|^2 < R^2$  indicates the  $\mathbf{u}_m$  is a vector within the convex uncertainty set.

Therefore, the convex uncertainty set can be obtained:

$$\left\{ \mathbf{u}_m \mid \|\phi(\mathbf{u}_m) - \mathbf{P}\|^2 \leq R^2, \forall m \right\} \quad (24)$$

In robust scheduling, due to the convexity of the constructed uncertainty set, it is only needed to ensure that the boundary support vectors satisfy the constraints.

## 2) Uncertainty Set Construction for the Industrial Site

The above analysis is at the mathematical level. In actual industrial sites, the application of PLK-based SVC technique may encounter new issues. For example, as claimed in Section IV-B-1),  $\mathbf{u}_m$  is a two-dimensional vector and its elements should have the same unit. However, this is not the case for  $U$  and  $T_{\text{amb}}$  in the scheduling of BTs.

To address this issue, this study defines the  $\mathbf{u}_m$  to consist of the variation of the bitumen temperature due to the variation of  $U$  and  $T_{\text{amb}}$ , i.e.,  $(\Delta T_{U_m}, \Delta T_{T_{\text{amb}}^m})$ , which is calculated as follows:

$$\Delta T_{U_m} = (U_m - U) \times \frac{A \times (T - T_{\text{amb}}) \times \Delta t}{c_v \times m} \quad (25)$$

$$\Delta T_{T_{\text{amb}}^m} = (T_{\text{amb}}^m - T_{\text{amb}}) \times \frac{U \times A \times \Delta t}{c_v \times m} \quad (26)$$

where  $U_m$  and  $T_{\text{amb}}^m$  are the  $m^{\text{th}}$  historical data of  $U$  and  $T_{\text{amb}}$ , respectively;  $\frac{A \times (T - T_{\text{amb}}) \times \Delta t}{c_v \times m}$  and  $\frac{U \times A \times \Delta t}{c_v \times m}$  are the partial

derivatives of the bitumen temperature with respect to  $U$  and  $T_{\text{amb}}$ , respectively, calculated from (5);  $\Delta T_{U_m}$  and  $\Delta T_{T_{\text{amb}}^m}$  are the

obtained elements for  $\mathbf{u}_m$  with the same unit ( $^{\circ}\text{C}$ ), which represent the temperature transfer deviation of BTs caused by the uncertainty of  $U_m$  and  $T_{\text{amb}}^m$ , respectively.

Subsequently, the data-driven SVC technique is used to generate the convex uncertainty set for scheduling BTs. Assuming the obtained boundary support vectors are denoted as

$\left\{ \Delta T_{U_q}, \Delta T_{T_{\text{amb}}^q} \right\}_{q=1}^Q$ , where  $Q$  is the number of boundary support

vectors, the corresponding historical data  $\left\{ U_q, T_{\text{amb}}^q \right\}_{q=1}^Q$  can be used for two-layer robust optimal scheduling.

## C. Two-Layer Robust Optimal Scheduling Model

The objective function of the upper-layer robust clustered optimization is the same as (7). The consideration of uncertain factors is mainly reflected in the constraints, which are provided as follows:

$$\bar{T}_h^q = \bar{T}_{h-1}^q + \frac{P_{\text{rate}} \times \frac{x_h}{N} - U_q \times A \times (\bar{T}_{h-1}^q - T_{\text{amb}}^q)}{c_v \times m} \times \Delta t, \forall q, \forall h \quad (27)$$

$$T_{\text{down}} + \Delta T \leq \bar{T}_h^q \leq T_{\text{up}} - \Delta T, \forall q, \forall h \quad (28)$$

It should be noted that, the actual  $U$  and  $T_{\text{amb}}$  vary at different times, while the fixed parameter values are utilized in both the deterministic optimal scheduling model and each scenario of the robust optimal scheduling model. If the temporal variation characteristics of  $U_q$  and  $T_{\text{amb}}^q$  are considered within each time slot, the dimension of the constructed uncertainty set should be  $2 \times H$ , resulting in too many scenarios to be considered in the robust model and making the computation more complex. In fact, the fixed values of  $U_q$  and  $T_{\text{amb}}^q$  in the uncertainty set can also achieve satisfactory performance in addressing the uncertainties of BTs in the robust model, as will be demonstrated in Section V-D.

Here concludes the formulation of the two-layer robust clustered optimization. Firstly, the SVC-based uncertainty set construction is executed considering robustness. Secondly, based on the obtained boundary support vectors of the constructed uncertainty set, the two-layer robust clustered optimization is implemented. The objective of the upper-layer robust clustered optimization is (7), which is subject to the constraints of (12), (27), and (28). After obtaining the number of BTs turned ON at each time slot considering uncertainties, the lower-layer state distribution is then executed. The objective of lower-layer state distribution is (11), subject to the constraints of (5), (6), and (10).

## V. CASE STUDY

In this section, the two-layer optimal scheduling model and the data-driven two-layer robust optimal scheduling model are applied to the industrial system introduced in Section II-A. All numerical simulations are conducted on a laptop equipped with a 2.60-GHz-i7 CPU processor and 8-GB RAM. The CPLEX solver is executed in MATLAB to solve the models.

The parameter values used in the cases are listed in Table I, sourced from real data provided by the KVM UK Ltd [4].

TABLE I  
PARAMETER VALUES

Parameter	Value	Parameter	Value	Parameter	Value
$U$ ( $\text{kWm}^{-2}\text{K}^{-1}$ )	$7.75 \times 10^{-3}$	$A$ ( $\text{m}^2$ )	36	$m$ (kg)	21500
$c_v$ ( $\text{kJkg}^{-1}\text{K}^{-1}$ )	1.34	$P_{\text{rate}}$ (kW)	120	$\Delta t$ (s)	900
$T_{\text{up}}$ ( $^{\circ}\text{C}$ )	180	$T_{\text{down}}$ ( $^{\circ}\text{C}$ )	150	$H$	96
$M$	400	/	/	/	/

## A. Deterministic Optimal Scheduling Results

In this subsection, different existing methods for solving the original optimal scheduling model, such as the CPLEX solver (with the optimality gap set at 0.01) and the PSO algorithm (with acceleration coefficients  $c1 = 1.8$ ,  $c2 = 2.2$ , and inertia weight  $w$

= 0.3), are compared with the proposed two-layer optimal scheduling model, which is also solved by the CPLEX solver with the same optimality gap. Moreover, the penalty function method is utilized in the PSO algorithm to handle the constraints.

TABLE II  
COMPARISON RESULTS OF DIFFERENT OPTIMAL SCHEDULING METHODS

Indices	$N$	Methods		
		CPLEX solver	PSO algorithm	Two-layer model
Calculation times (s)	10	214.38	6627.23	13.27
	15	968.47	18223.71	13.92
	20	7359.65	/	13.46
Peak-to-valley differences (MW)	10	0.3872	0.4335	0.4221
	15	0.1552	0.1871	0.1934
	20	0.1136	/	0.1136

Table II presents the comparison results of different optimal scheduling methods for  $N = 10, 15,$  and  $20,$  respectively. In terms of computation times, the CPLEX solver outperforms the PSO algorithm when solving the original optimal scheduling model. Nevertheless, when  $N = 20,$  the calculation time of the CPLEX solver exceeds 2 hours, which is difficult to execute in actual industrial processes (e.g., in a receding horizon control manner). The calculation times of the two-layer optimal scheduling model indicate that it not only has a much faster computation speed but also remains unaffected by the increasing scale of BTs.

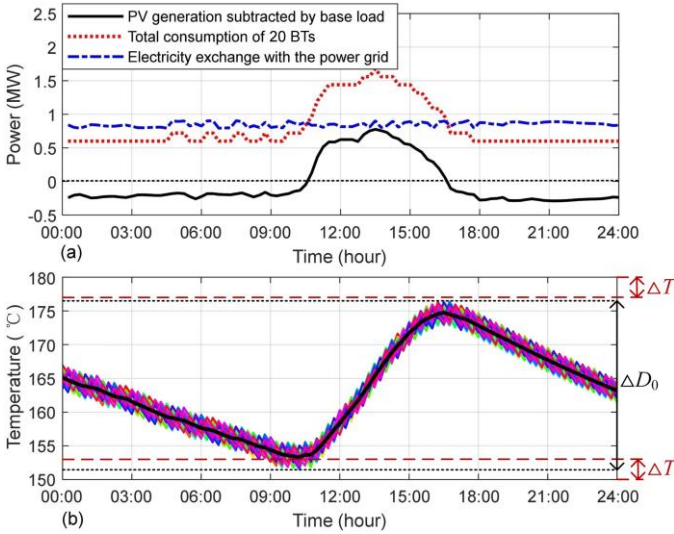


Fig. 4. (a) Two-layer deterministic optimal scheduling results of 20 BTs and (b) the corresponding temperature transfer process.

The two-layer deterministic optimal scheduling results and the corresponding temperature transfer process of BTs when  $N = 20$  are provided in Fig. 4. Fig. 4(a) depicts the shape of the total consumption curve of 20 BTs, which is approximately consistent with the curve of net PV generation (PV generation subtracted by base load). Additionally, the curve of the power exchange with the main grid is almost flat, achieving the scheduling objective of minimizing the peak-to-valley difference. Fig. 4(b) exhibits the temperature transfer process of BTs. Each colored curve in Fig. 4(b) represents the temperature fluctuation of a BT. Meanwhile, the average temperature curve (represented by the black line) and the magnitude of the gap  $\Delta T$  are also exhibited in Fig. 4(b). Between approximately 10:00 and 16:30, the average temperature of BTs is increasing, which coincides

with a relatively higher power consumption of BTs during this period. On the contrary, during other periods, the decreasing average temperature of BTs coincides with relatively lower power consumption values. The  $\Delta D_0$  in Fig. 4(b) shows the difference of the maximum and minimum temperatures of BTs during the entire temperature transfer process. Table II shows that, when  $N = 20,$  the two-layer optimal scheduling achieves the same peak-to-valley difference as the original optimal scheduling model. However, when  $N = 10$  and  $N = 15,$  the two-layer optimal scheduling model achieves inferior peak-to-valley differences compared to the original optimal scheduling model. Moreover, as indicated in Table II, the peak-to-valley difference increases as  $N$  decreases. The reasons are analyzed below.

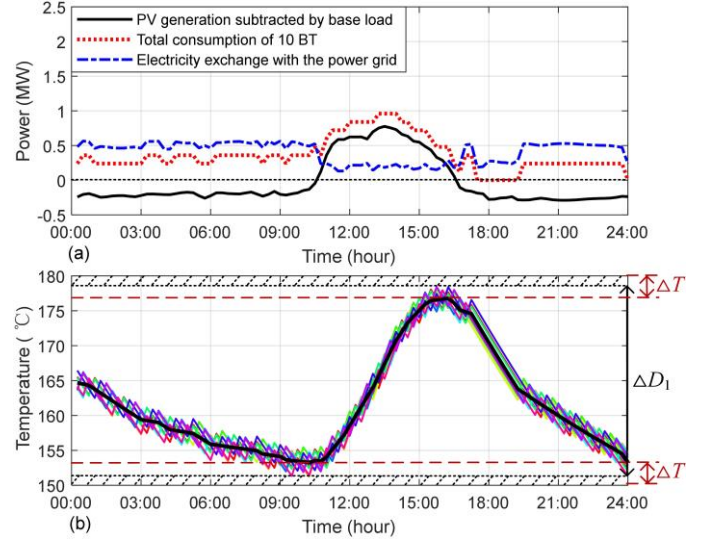


Fig. 5. (a) Two-layer deterministic optimal scheduling results of 10 BTs and (b) the corresponding temperature transfer process.

Fig. 5 depicts the two-layer deterministic optimal scheduling results and the corresponding temperature transfer process of 10 BTs. Due to the limited scheduling capacity of 10 BTs, the curve of the electricity exchange with the power grid (illustrated in Fig. 5(a)) exhibits a larger peak-to-valley difference than that in Fig. 4(a). Moreover, according to (9), the average temperature curve of BTs in the two-layer optimal scheduling results is confined between the dashed red lines. This leads to the temperature variation curve of each BT not being able to fall within the region of dashed black lines in Fig. 5(b). Thus, the temperature variation space of BTs in the two-layer model is a little smaller than the original optimal scheduling model, resulting in an inferior result in the peak-to-valley difference. Nevertheless, the gap in peak-to-valley difference between these two models is only 0.0349 MW, which is certainly industrially acceptable given the significant drop in computing duration. Similar analysis can be applied to the optimal scheduling results when  $N = 15,$  which is not provided here.

### B. Influence of Uncertain Factors

Due to the influence of uncertain factors, the day-ahead two-layer deterministic optimal schedule ( $x_{i,h}$ ) of BTs may lead to constraint violation. Fig. 6 depicts the empirical  $U$  and the forecasted  $T_{amb}$  on a rainy day, along with their respective actual

values. On this day, the actual values of  $U$  are higher than the empirical value due to the wet weather.

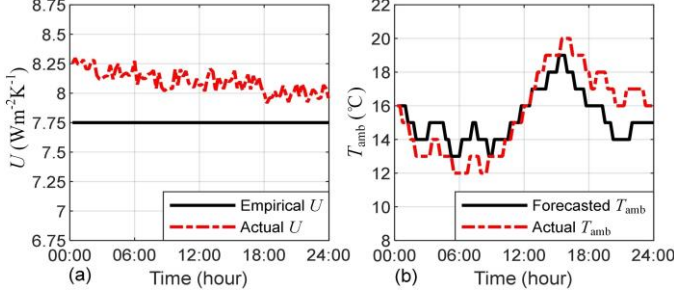


Fig. 6. (a) The empirical  $U$  and (b) the forecasted  $T_{\text{amb}}$  on a rainy day.

Fig. 7(a) illustrates the actual execution results of 20 BTs on this day, which are based on the day-ahead schedule obtained by the two-layer deterministic optimal scheduling model. Fig. 7(b) displays the actual temperature variations of BTs. In the actual scenario depicted in Fig. 6, due to the higher  $U$  and lower  $T_{\text{amb}}$  before approximately 09:00, the heat of BTs dissipates faster than expected. Therefore, the actual temperatures of BTs drop more rapidly compared to the day-ahead scheduling results (as illustrated in Fig. 4(b)), leading to the temperatures of BTs approaching  $T_{\text{down}}$  at about 09:00 (as shown in Fig. 7(b)). The electrical heater of some BTs automatically turns ON when their temperatures reach the  $T_{\text{down}}$ , leading to obvious fluctuations during the following period in the actual power consumption curve of BTs, as circled in Fig. 7(a).

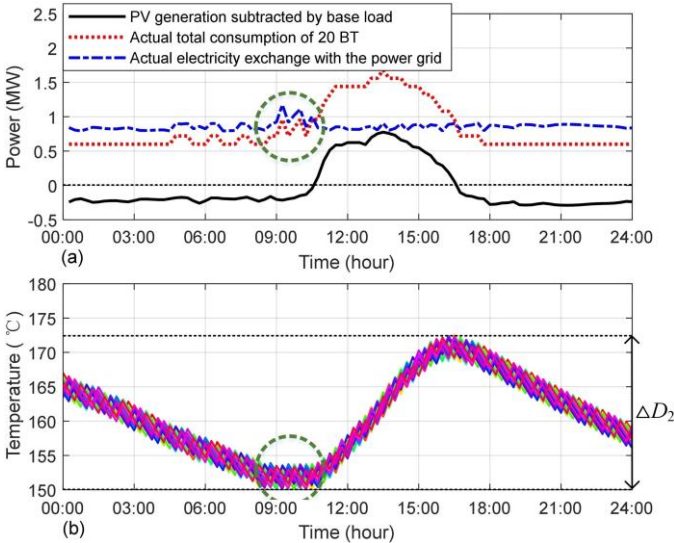


Fig. 7. (a) Actual execution results of the schedule of 20 BTs obtained by the two-layer deterministic model under the uncertainty and (b) the corresponding temperature transfer process.

### C. Generation of Uncertainty Sets

In this study, 400 historical data samples of  $\mathbf{u}_m$  are collected from the KVM UK Ltd [4] and shown in Fig. 8. From Fig. 8, it can be seen that the uncertainty in  $U$  may cause a maximum deviation in the bitumen temperature of about  $0.188^{\circ}\text{C}$  per  $\Delta t = 15$  min, while the uncertainty in  $T_{\text{amb}}$  may result in a maximum deviation of about  $0.034^{\circ}\text{C}$  per  $\Delta t$ . This implies that compared to the uncertainty in  $T_{\text{amb}}$ , the uncertainty in  $U$  is likely to cause more deviations in the bitumen temperature. If these uncertain

factors are not effectively considered in the day-ahead optimal scheduling model, they could lead to accumulated temperature deviations in actual execution (as illustrated in Fig. 7(b)). For example, on a rainy day, the rain may last for several hours (e.g., 6 hours). During this rainy period, the higher  $U$  can lead to the accumulated temperature deviation reaching  $(0.188 \times 24) = 4.512^{\circ}\text{C}$ . Considering that the allowable temperature range of BTs is from  $150^{\circ}\text{C}$  to  $180^{\circ}\text{C}$ , this accumulated temperature deviation is notable and may cause the bitumen temperature go beyond the allowable range. If that happens, the BTs, detecting this deviation via temperature sensors, would have to move away from the original optimal schedule to correct the bitumen temperature back to the allowable range, thus leading to larger power fluctuations of BTs, as analyzed in Section V-B.

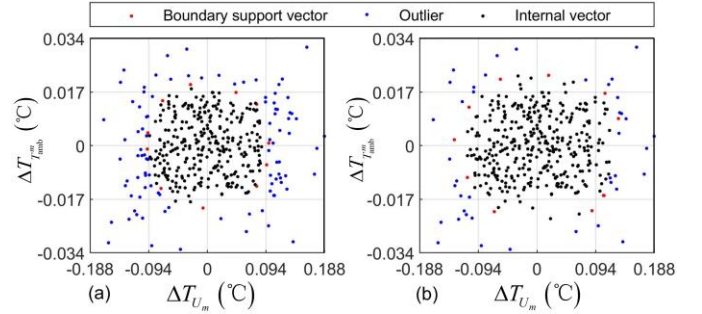
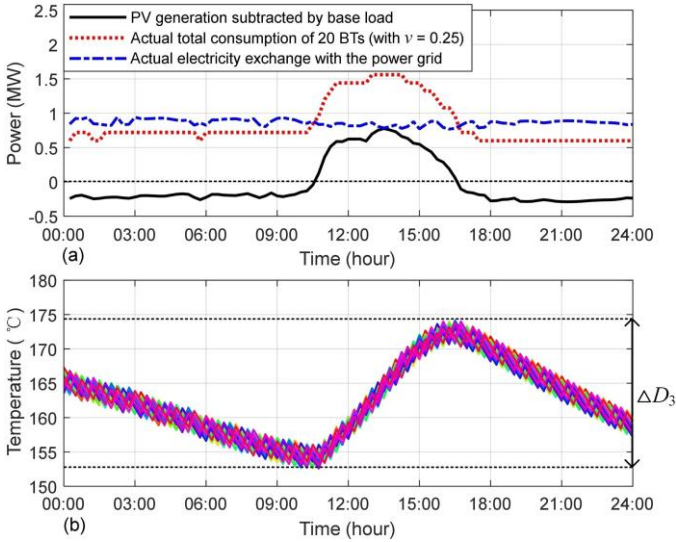


Fig. 8. Uncertainty sets of  $\mathbf{u}_m$  with (a)  $\nu = 0.25$  and (b)  $\nu = 0.125$ .

Fig. 8 illustrates the generated uncertainty sets by using the PLK-based SVC technique. The conservatism of the uncertainty set can be increased by reducing the regularization parameter  $\nu$ , as introduced in (13). In Fig. 8, the red points represent the boundary support vectors of the uncertainty set, the blue points represent the outliers, and the black points represent the vectors within the uncertainty set. Through utilizing the boundary support vectors in the two-layer robust optimization, the influence of uncertain factors in the actual execution of day-ahead robust scheduling of BTs can be considered.

### D. Two-layer Robust Optimal Scheduling Results

The actually executed power consumption curve of 20 BTs based on the two-layer robust optimal scheduling (with  $\nu = 0.25$ ) is illustrated in Fig. 9(a). By considering the uncertainty set in the two-layer robust model, no BT is unexpectedly turned ON or OFF during the actual temperature transfer process, as shown in Fig. 9(b).



**Fig. 9.** (a) Actual execution results of two-layer robust optimal scheduling (with  $\nu = 0.25$ ) of 20 BTs and (b) the corresponding temperature transfer process.

It is noteworthy that in the two-layer robust model, due to the consideration of the uncertainty set, the temperature difference,  $\Delta D_3$  (shown in Fig. 9(b)), is reduced compared to  $\Delta D_0$  (shown in Fig. 4(b)). This is because, to avoid violating the temperature limits in actual scenarios, the day-ahead two-layer robust optimization results turn ON more BTs before approximately 10:00, and more BTs are turned OFF between approximately 10:00 and 16:30.

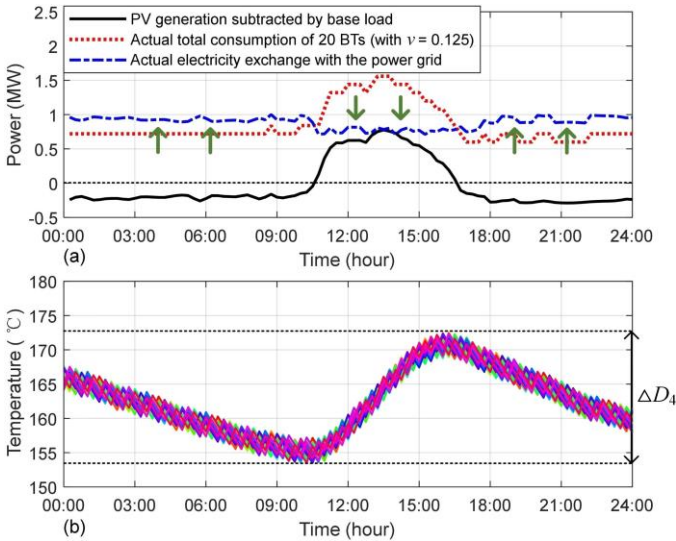


**Fig. 10.** (a) Actual execution results of two-layer robust optimal scheduling (with  $\nu = 0.125$ ) of 20 BTs and (b) the corresponding temperature transfer process.

Fig. 10(a) gives the actually executed power consumption curve of 20 BTs based on the day-ahead two-layer robust optimal scheduling (with  $\nu = 0.125$ ). In this case, the conservatism of the uncertainty set is further increased compared to  $\nu = 0.25$ , leading to a further reduction in the temperature difference,  $\Delta D_4$ , compared to  $\Delta D_3$ . Consequently, more BTs are turned ON before approximately 10:00, and more are turned OFF between approximately 10:00 and 16:30. As a result, the actual electricity demand from the power grid obtained by the day-ahead two-layer robust model with  $\nu = 0.125$  is higher

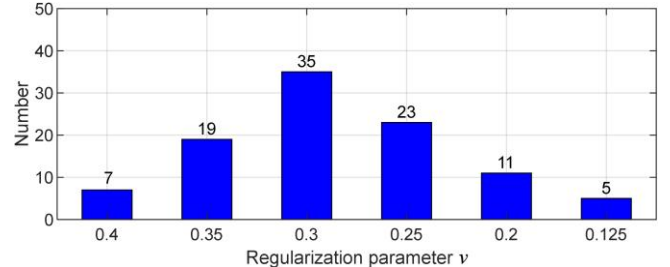
than that with  $\nu = 0.25$  before approximately 10:00 and is lower than that between approximately 10:00 and 16:30.

TABLE III  
COMPARISON OF ACTUAL PEAK-TO-VALLEY DIFFERENCES

Two-layer optimal scheduling model	Peak-to-valley difference (MW)
Deterministic model	0.3820
Robust model (with $\nu = 0.4$ )	0.2181
Robust model (with $\nu = 0.35$ )	0.1847
Robust model (with $\nu = 0.3$ )	0.1695
Robust model (with $\nu = 0.25$ )	0.1741
Robust model (with $\nu = 0.2$ )	0.2208
Robust model (with $\nu = 0.125$ )	0.2914
Robust model (with an ellipse as the uncertainty set)	0.4003
Robust model (with a box as the uncertainty set)	0.4198

Table III compares the actual peak-to-valley difference rates of two-layer robust optimal scheduling model under different levels of conservatism. When the ellipse is treated as the uncertainty set, the least squares method is employed to form an elliptical region that covers all historical data samples. Moreover, when the box is treated as the uncertainty set, the maximum and minimum values of  $\{\mathbf{u}_m\}_{m=1}^M$  in each dimension are considered as the boundaries of the box. Due to the traditional uncertainty sets (ellipse and box) covering all historical data samples, they are more conservative than the uncertainty sets generated by using the PLK-based SVC technique. Therefore, initially, with an increase in conservatism (decrease in  $\nu$ ), the actual peak-to-valley difference decreases. However, as conservatism further increases (e.g., when  $\nu = 0.125$  or when the ellipse or box is used as the uncertainty set), the peak-to-valley characteristic gradually deteriorates due to over-conservatism. The comparison results show that when  $\nu = 0.3$ , it is an appropriate level of conservatism that enables the proposed two-layer robust model to achieve a better actual peak-to-valley difference.

Remark: all of the above two-layer robust models of BTs are executed under a specific actual scenario depicted in Fig. 6. To obtain the most suitable level of conservatism for the two-layer robust model, it is needed to examine its performance across various actual scenarios.



**Fig. 11.** Number of actual scenarios achieving a better peak-to-valley difference under the two-layer robust model with different values of  $\nu$ .

In this study, 100 historical data samples are randomly selected from the 400 samples depicted in Fig. 8. Then, the performance of two-layer robust model with different values of  $\nu$  is examined for various actual scenarios corresponding to the selected samples. In general, a robust model with lower conservatism exhibits superior performance in scenarios with

lower uncertainty; conversely, it performs better in scenarios with higher uncertainty when featuring higher conservatism. Fig. 11 illustrates that the two-layer robust model with  $\nu = 0.3$  outperforms other values of  $\nu$  in 35 out of 100 actual scenarios, making it the recommended choice in this study.

## VI. CONCLUSION

In this article, a two-layer robust optimal scheduling model is proposed for tapping the flexibility contained in IHLs. To deal with the great calculation difficulty and uncertainties, the clustered temperature transfer process of BTs is investigated, and a data-driven PLK-based SVC technique is utilized to deal with the uncertainties in robust optimal scheduling. Compared with the original optimal scheduling model, the proposed two-layer optimal scheduling model can largely reduce the computation time of scheduling 20 BTs from over 2 hours to 13.46s, with both models being solved using the CPLEX solver. Moreover, by comparing the results of two-layer robust model in various actual scenarios, a recommended level of conservatism ( $\nu = 0.3$ ) is adopted to mitigate the influence of uncertain factors in the actual execution of day-ahead schedules.

The appropriate conservatism of the two-layer robust model varies across various actual scenarios (as shown in Fig. 11), and the characteristics of actual scenarios are correlated with external weather conditions. Therefore, combining the local weather monitoring system to establish an adaptive conservatism adjustment strategy may further enhance the effectiveness of the day-ahead two-layer robust model, which is considered a direction for future research. Moreover, given that BTs are equipped with real-time temperature sensors, it is possible to iteratively correct the accumulated temperature deviation of BTs within a receding-horizon framework (e.g., real-time predictive control). This presents another promising direction for future research.

## VII. REFERENCES

- [1] R. Hanna and D. G. Victor, "Marking the decarbonization revolutions," *Nature Energy*, vol. 6, no. 6, pp. 568-571, 2021.
- [2] C. Dang, J. Zhang, C.-P. Kwong *et al.*, "Demand side load management for big industrial energy users under blockchain-based peer-to-peer electricity market," *IEEE Transactions on Smart Grid*, vol. 10, no. 6, pp. 6426-6435, 2019.
- [3] "Bitumen Market Size, 2022 to 2032". [Online]. Available at <https://www.precedenceresearch.com/bitumen-market>.
- [4] "Market Changes Reflected in Latest UK Asphalt Industry Report". [Online]. Available: <https://www.asphaltuk.org/key-facts/>.
- [5] "How is Bitumen Heated?". [Online]. Available: <https://teccontainersolutions.com/2022/12/how-is-bitumen-heated/>.
- [6] "MBA Asphalt Plants". [Online]. Available at <https://mbaplant.com/en/asphalt-plant/>.
- [7] X. Xiao, D. Cai, L. Lou *et al.*, "Application of asphalt based materials in railway systems: A review," *Construction and Building Materials*, vol. 304, p. 124630, 2021.
- [8] Y. Zhou, M. Cheng, and J. Wu, "Enhanced frequency response from industrial heating loads for electric power systems," *IEEE Transactions on Industrial Informatics*, vol. 15, no. 6, pp. 3388-3399, 2018.
- [9] M. Cheng, J. Wu, S. J. Galsworthy *et al.*, "Power system frequency response from the control of bitumen tanks," *IEEE Transactions on Power Systems*, vol. 31, no. 3, pp. 1769-1778, 2015.
- [10] C. Wu, H. Han, S. Gao *et al.*, "Coordinated Scheduling for Multi-Microgrid Systems Considering Mobile Energy Storage Characteristics of Electric Vehicles," *IEEE Transactions on Transportation Electrification*, 2022.
- [11] F. Verastegui, A. Lorca, D. E. Olivares *et al.*, "An adaptive robust optimization model for power systems planning with operational uncertainty," *IEEE Transactions on Power Systems*, vol. 34, no. 6, pp. 4606-4616, 2019.
- [12] A. Hamed, E. Shaban, R. Darwish *et al.*, "Design and implementation of discrete PID control applied to Bitumen tank based on new approach of pole placement technique," *International Journal of Dynamics and Control*, vol. 5, pp. 604-613, 2017.
- [13] A. Testa, A. Rucco, and G. Notarstefano, "Distributed mixed-integer linear programming via cut generation and constraint exchange," *IEEE Transactions on Automatic Control*, vol. 65, no. 4, pp. 1456-1467, 2019.
- [14] F. Najafi and M. Fripp, "Stochastic optimization of comfort-centered model of electrical water heater using mixed integer linear programming," *Sustainable Energy Technologies and Assessments*, vol. 42, p. 100834, 2020.
- [15] M. A. Bragin and E. L. Tucker, "Surrogate "Level-Based" Lagrangian Relaxation for mixed-integer linear programming," *Scientific Reports*, vol. 12, no. 1, p. 22417, 2022.
- [16] C. Wu, S. Jiang, S. Gao *et al.*, "Event-triggered model predictive control for dynamic energy management of electric vehicles in microgrids," *Journal of Cleaner Production*, vol. 368, p. 133175, 2022.
- [17] K. Amine, "Multiobjective simulated annealing: Principles and algorithm variants," *Advances in Operations Research*, vol. 2019, 2019.
- [18] M. Elkazaz, M. Sumner, E. Naghiyev *et al.*, "A hierarchical two-stage energy management for a home microgrid using model predictive and real-time controllers," *Applied Energy*, vol. 269, p. 115118, 2020.
- [19] C. Wu, H. Han, S. Gao *et al.*, "Coordinated Scheduling for Multimicrogrid Systems Considering Mobile Energy Storage Characteristics of Electric Vehicles," *IEEE Transactions on Transportation Electrification*, vol. 9, no. 1, pp. 1775-1783, 2022.
- [20] X. Wu, L. You, R. Wu *et al.*, "Management and Control of Load Clusters for Ancillary Services Using Internet of Electric Loads Based on Cloud-Edge-End Distributed Computing," *IEEE Internet of Things Journal*, vol. 9, no. 19, pp. 18267-18279, 2022.
- [21] R. Pereira, A. Fagundes, R. Melício *et al.*, "A fuzzy clustering approach to a demand response model," *International Journal of Electrical Power & Energy Systems*, vol. 81, pp. 184-192, 2016.
- [22] B. Zhao, T. Qian, W. Tang *et al.*, "A data-enhanced distributionally robust optimization method for economic dispatch of integrated electricity and natural gas systems with wind uncertainty," *Energy*, vol. 243, p. 123113, 2022.
- [23] M. Zhang, J. Fang, X. Ai *et al.*, "Partition-combine uncertainty set for robust unit commitment," *IEEE Transactions on Power Systems*, vol. 35, no. 4, pp. 3266-3269, 2020.
- [24] H. Daneshvari and R. Shafaei, "A new correlated polyhedral uncertainty set for robust optimization," *Computers & Industrial Engineering*, vol. 157, p. 107346, 2021.
- [25] D. Bertsimas and M. Sim, "The price of robustness," *Operations research*, vol. 52, no. 1, pp. 35-53, 2004.
- [26] A. Ben-Hur, D. Horn, H. T. Siegelmann *et al.*, "Support vector clustering," *Journal of machine learning research*, vol. 2, no. Dec, pp. 125-137, 2001.
- [27] P. Qiu, "A jump-preserving curve fitting procedure based on local piecewise-linear kernel estimation," *Journal of Nonparametric Statistics*, vol. 15, no. 4-5, pp. 437-453, 2003.
- [28] C. Shang, X. Huang, and F. You, "Data-driven robust optimization based on kernel learning," *Computers & Chemical Engineering*, vol. 106, pp. 464-479, 2017.
- [29] S. Liang, X. Zeng, and Y. Hong, "Distributed nonsmooth optimization with coupled inequality constraints via modified Lagrangian function," *IEEE Transactions on Automatic Control*, vol. 63, no. 6, pp. 1753-1759, 2017.
- [30] A. Sinha, T. Soun, and K. Deb, "Using Karush-Kuhn-Tucker proximity measure for solving bilevel optimization problems," *Swarm and evolutionary computation*, vol. 44, pp. 496-510, 2019.
- [31] H. Zhu, F. Ye, and E. Zhou, "Solving the dual problems of dynamic programs via regression," *IEEE Transactions on Automatic Control*, vol. 63, no. 5, pp. 1340-1355, 2017.
- [32] D. A. Pisher and D. M. Schryer, "Support vector machine," in *Machine learning*: Elsevier, 2020, pp. 101-121.
- [33] M. Shao, X. Wang, Z. Bu *et al.*, "Prediction of energy consumption

in hotel buildings via support vector machines," *Sustainable Cities and Society*, vol. 57, p. 102128, 2020.

**Chuanshen Wu** received the B.S. degree from Fuzhou University, Fuzhou, China, in 2015, and the Ph.D. degree from Southeast University, Nanjing, Jiangsu, China, in 2022, both in Electrical Engineering. He is currently a Research Associate with the School of Engineering, Cardiff University, Cardiff, U.K. His research interests include demand-side response, integrated energy system operation and planning, uncertain analysis, and electric vehicle integration.

**Yue Zhou** received the B.Eng. and Ph.D. degrees in Electrical Engineering in Tianjin University in 2011 and 2016, respectively. From 2017 to 2020, he worked as a Postdoctoral Research Associate at School of Engineering at Cardiff University, Wales, UK. Since April 2020, he has become a Lecturer in Cyber Physical Systems at School of Engineering at Cardiff University, Wales, UK. His research interests lie around cyber physical energy systems, specifically including demand side response, peer-to-peer energy trading, distributed ledger technology and smart local energy systems.

**Jianzhong Wu** received the B.Sc., M.Sc., and Ph.D. degrees in Electrical Engineering from Tianjin University, China, in 1999, 2002, and 2004, respectively. He is Professor of Multi-vector Energy Systems and the Head of the School of Engineering, Cardiff University, UK. His research interests include integrated multienergy infrastructure and smart grid.